

This is the accepted manuscript made available via CHORUS. The article has been published as:

Evolution of nontrivial Fermi surface features in the band structures of the homologous members

$\text{Pb}_{\{5\}}\text{Bi}_{\{6\}}\text{Se}_{\{14\}}$ and $\text{Pb}_{\{5\}}\text{Bi}_{\{12\}}\text{Se}_{\{23\}}$

D. Koumoulis, L. Fang, D. Y. Chung, M. G. Kanatzidis, and L.-S. Bouchard

Phys. Rev. B **101**, 115309 — Published 30 March 2020

DOI: [10.1103/PhysRevB.101.115309](https://doi.org/10.1103/PhysRevB.101.115309)

Evolution of non-trivial Fermi Surface Features in the Band Structures of Homologous Members $\text{Pb}_5\text{Bi}_6\text{Se}_{14}$ and $\text{Pb}_5\text{Bi}_{12}\text{Se}_{23}$

D. Koumoulis,^{1,*} L. Fang,² D. Y. Chung,³ M.G. Kanatzidis,^{2,3,*} L.-S. Bouchard^{1,4,*}

¹Department of Chemistry and Biochemistry, University of California, Los Angeles, CA 90095-1569 USA

²Department of Chemistry, Northwestern University, Evanston, Illinois 60208, USA

³Division of Materials Sciences, Argonne National Laboratory US DOE, Argonne, Illinois 60439, USA

⁴California NanoSystems Institute, UCLA, Los Angeles, CA 90095 USA

ABSTRACT

High quality single crystals of $(\text{PbSe})_5(\text{Bi}_2\text{Se}_3)_{3m}$ were grown and analyzed by nuclear magnetic resonance (NMR) spectroscopy. We report on ^{77}Se and ^{207}Pb NMR shifts and nuclear spin-lattice relaxation measurements in the naturally formed heterostructure homology $(\text{PbSe})_5(\text{Bi}_2\text{Se}_3)_{3m}$ with $m=1$ ($\text{Pb}_5\text{Bi}_6\text{Se}_{14}$) and $m=2$ ($\text{Pb}_5\text{Bi}_{12}\text{Se}_{23}$). A distinct site-specific contribution has been detected for both nuclei as function of temperature, which reveals an electronic changeover from a semiconducting $\text{Pb}_5\text{Bi}_6\text{Se}_{14}$ to a semimetallic-like $\text{Pb}_5\text{Bi}_{12}\text{Se}_{23}$ system with nontrivial band structure features near the Fermi level. The temperature dependences of the relaxation rates are dominated by significant changes in the topology of energy dispersions accompanied with band edges and crossings in the region of the Fermi surface. These results, which interrogate nuclear-spin interactions from selected atomic sites, clearly expose the effects of the added Bi_2Se_3 layer on the crystal

and electronic structure of $\text{Pb}_5\text{Bi}_{12}\text{Se}_{23}$. These findings provide direct microscopic insight into the unconventional and dual nature of the electronic structure of these homologous thermoelectric and topologically nontrivial compounds.

KEYWORDS: *crystal structure, homologous compounds, electronic band gap, Fermi surface, heterostructure, NMR*

I. INTRODUCTION

The design and synthesis of advanced topological insulating materials for novel efficient thermoelectric [1] and optoelectronic properties [2] is currently of high interest in solid-state chemistry and materials engineering. It requires the design of low-cost and highly efficient materials that can enable conversion (via a solid state process) of heat into electricity by showing enhanced carrier mobility accompanied with low lattice thermal conductivity, as well as exhibit optical properties such as field-effect transistors (FETs)[2]. In this work, a naturally formed heterostructured material is comprised of alternating layers of PbSe and Bi_2Se_3 , as expressed by the homologous formula $(\text{PbSe})_5(\text{Bi}_2\text{Se}_3)_{3m}$, where $m=1,2$ [1,3] has been studied. This homologous series combines two prototype materials: PbSe, a well-studied thermoelectric (TE) and Bi_2Se_3 , a prototypical topological insulator (TI) material. As a result, a multi-functional material with dual properties is expected. The value of m designates the number of Bi_2Se_3 sheets that are sandwiched by consecutive PbSe slabs. The Bi_2Se_3 sheet is hexagonal and is identical to a quintuple layer (QL) of the topological insulator Bi_2Se_3 . The PbSe sheet has tetragonal symmetry and is a two-atom thick slice from the face-centered-cubic (FCC) structured PbSe. The lattice mismatch between Bi_2Se_3 and PbSe produces a stress that strongly distorts the slab of PbSe along the c -axis for both homologous phases. Regarding the band structure characteristics of this series, Nakayama *et al.* [4] provided experimental evidence for the existence of a dramatic change in the electronic states character around the Fermi energy related to an upgraded band inversion (BI) process associated with a three-dimensional (3D) to two-dimensional (2D) crossover due to the layering symmetry of the $(\text{PbSe})_5(\text{Bi}_2\text{Se}_3)_{3m}$ series [4]. Band inversion plays a key role in the alteration of the topological order [4,5] through

a band splitting originating mainly by the strong spin-orbit coupling as well as lattice distortions and defects [4,5,6]. As originally proposed by Dimmock *et al.* [7], during the BI process a band gap evolution takes place upon doping through a systematic closing and gradual reopening of the gap between the conduction and valence bands. As a result, there is an inverted band symmetry related to the former (e.g. $\text{Pb}_x\text{Sn}_{1-x}\text{Te}$ [6,7], $(\text{PbSe})_5(\text{Bi}_2\text{Se}_3)_{3m}$ [4,8] etc.). Scalar relativistic, electronic and structural terms are essential contributions to the BI mechanism. Furthermore, the $m=1$ phase features a large number of chemical bonds with a length of $\sim 3.25 \text{ \AA}$ between the PbSe and Bi_2Se_3 sheets, creating a 3D structure. In the $m=2$ phase, the two adjacent QLs II and III are connected by van der Waals bonding. This weak bonding relaxes the stress and preserves the uniformity of the Bi_2Se_3 sheets. Crystal cleaving always occurs along the van der Waals plane and exposes an ideal surface of Bi_2Se_3 with Dirac Fermions residing on it. By contrast, crystal cleavage in the $m=1$ phase breaks the chemical bonding between PbSe and Bi_2Se_3 , likely leaving a large number of dangling bonds on top of the Bi_2Se_3 slab.

An angle-resolved photoemission spectroscopy (ARPES) study on $m=1$ and $m=2$ phases by Nakayama *et al.* [4] and first-principles calculations by Momida *et al.* [8] have shown a marked difference on the band dispersions near the Fermi level (E_F) in these two samples. Namely, the band structure for $m=1$ is a single parabolic band, whereas for $m=2$ the band structure consists of multiple bands associated with a shallow dip at the top due to the presence of additional bands that cross E_F . The $m=2$ sample has a more complicated band structure than $m=1$. The presence of a large gap of approximately 0.5 eV in the topological states as well as the even number of E_F crossings of the bands indicate that the $m=2$ sample cannot be classified within the framework of known topological insulating materials. In particular, ARPES experiments on $m=2$ [4] revealed six dispersive features around the near- E_F region where two of them cross E_F and overlap with the Dirac-cone surface states, which mainly originate from the Bi_2Se_3 layers. Recent *ab initio* calculations [8] for the $m=2$ system have shown that its electronic structure near the Fermi energy consists of a mixture of Bi_2Se_3 - and PbSe-layer bands.

Herein we report results of a combined ^{77}Se and ^{207}Pb NMR investigation carried out on $\text{Pb}_5\text{Bi}_6\text{Se}_{14}$ ($m=1$) and $\text{Pb}_5\text{Bi}_{12}\text{Se}_{23}$ ($m=2$) to explore at the microscopic level the unusual electronic features that have been predicted from band structures calculations performed on $(\text{PbSe})_5(\text{Bi}_2\text{Se}_3)_{3m}$. During the BI process that arises from a continuous transition from $m=1$ to $m=2$, ^{207}Pb and ^{77}Se NMR spectra as well as nuclear spin-lattice relaxation rates (variable temperature) provide electronic characterization of the electronic energy bands that cross or lie near the Fermi level [6,9, 10,11], and provided a better understanding of the topologically nontrivial features of the Fermi level density of states for $(\text{PbSe})_5(\text{Bi}_2\text{Se}_3)_{3m}$.

II. EXPERIMENTAL SECTION

A ground powder mixture (total 5 g scale) of PbSe and Bi_2Se_3 with a stoichiometric ratio for $m=1$ and $m=2$ was loaded in a silica-fused tube (12 mm OD) and sealed under vacuum at 10^{-4} mbar. The mixture was melted at 750°C for 1 h, followed by slow cooling at 2°C/h to room temperature. The respective synthesis for $m=1$ and $m=2$ produced single crystal whiskers and an ingot. Thermopower measurements were performed on the polycrystalline pellet samples. The pellet samples were prepared by sintering a stoichiometric mixture of fine powder of PbSe and Bi_2Se_3 to prevent the formation of second phases that can form above the melting points (744°C for $m=1$ and 690°C for $m=2$) of the compounds by peritectic decomposition. The synthesis was processed at 600°C and 550°C for $m=1$ and $m=2$, respectively, for 10 days and produced agglomerates of the target compound at a quantitative yield of nearly pure phase. The sample for thermopower was prepared by cold-press and annealing at 500°C for 3 days. The measured density of the pellet samples was about 97% of the calculated value. We confirmed that the anisotropic effect of thermopower on these compounds is very small at room temperature [12]. The carrier density of our samples was not measured and cannot be evaluated directly from that of the Sassi *et al.* [13] compound with $m=2$ because of different doping levels of the samples prepared in different conditions. However, we speculate that the carrier density is in the same order of magnitude as their thermopowers are in a narrow range from -50 to $-30\ \mu\text{V/K}$. Also, the carrier density of the compound $m=1$ may be lower than that of the $m=2$ compound based on the thermopower data on the samples prepared under the same

conditions. More details about the synthesis procedure and characterization of the homologous $(\text{PbSe})_5(\text{Bi}_2\text{Se}_3)_{3m}$ series can be found in Refs. [1,3]. The NMR measurements were performed on a Bruker DSX-300 spectrometer operating at a frequency of 62.79 MHz for lead (^{207}Pb) and 57.24 MHz for selenium (^{77}Se) nuclei [14,15,16]. The chemical shift scales were calibrated using the \mathcal{E} scale [12], where the reference compounds for defining 0 ppm on the chemical shift scales were the tetramethyllead (^{207}Pb) and dimethylselenide (^{77}Se) [14]. Static polycrystalline samples of $\text{Pb}_5\text{Bi}_6\text{Se}_{14}$ ($m=1$) and $\text{Pb}_5\text{Bi}_{12}\text{Se}_{23}$ ($m=2$) were placed in a 5-mm solenoid coil of a standard Bruker X-nucleus NMR probe. All samples were ground with a mortar and pestle to reduce radiofrequency (RF) skin-depth effects at these NMR frequencies. The ^{207}Pb $\pi/2$ pulse width was 4.5 μs . The ^{77}Se $\pi/2$ pulse width was 4.0 μs . Spectral (lineshape) data were acquired using a spin-echo sequence $[(\pi/2)_x - \tau - (\pi)_y - \tau - \text{acquire}]$ with the echo delay, τ , set to 20 μs . Nuclear spin-lattice relaxation times (T_1) were measured with a saturation recovery technique for both ^{77}Se and ^{207}Pb nuclei for all samples [15,16].

III. RESULTS AND DISCUSSION

Numerous studies have shown that NMR static and dynamic parameters can probe the coupling of specific lattice site nuclei to the electronic band charge carriers, as well as to the quadrupolar effects [15,16,17,6,18,19,9,18-35]. This is a (selective) site-specific benefit of NMR spectroscopy compared to other techniques, which can be used to probe the involvement of local orbitals and hybridization effects in the conduction process. Since 2012 [21,31] there have been many demonstrations via NMR experiments and theoretical analyses [25,27] of the usefulness of the NMR frequency shift at probing strong relativistic effects as well as unusual electronic characteristics and band features of TI and TE materials. The aforementioned sensitivity to relativistic effects (e.g. spin-orbit coupling) due to the presence of heavy Z-elements in alloys is an essential parameter for manifestation of the BI effect. The BI depends on the nature of the charge carrier, charge carrier and/or lattice defect density (as well as impurities), and electronic inhomogeneities [15,21,30,31,35]. All the aforementioned parameters can be detected via the nuclear spin-lattice relaxation mechanism and Knight shift [16,19,9], using sensitive atomic level probes

that can accurately assess the *s*- or non-*s* electron nature at the density of states at the Fermi level [36-38,9,35,39,40].

Figure 1 presents the static ^{77}Se NMR spectra of two powdered samples $(\text{PbSe})_5(\text{Bi}_2\text{Se}_3)_{3m}$, $m=1,2$ at ambient temperature (296 K). For both samples, a single resonance was observed. Both spectra are well described by a Gaussian lineshape. The $m=1$ sample shows the ^{77}Se resonance at -98.05 ppm, while for $m=2$ it lies at -16.69 ppm. A detailed study via ^{77}Se NMR on PbSe and Bi_2Se_3 can be found in Ref. [15] and Refs. [31,32,33,41], respectively. Recently, comprehensive ^{77}Se NMR studies on single crystals of Bi_2Se_3 revealed the presence of non-equivalent crystallographic Se sites in the spectra with the crystallographic *c*-axis parallel and perpendicular to the external magnetic field [32,33,41]. When dealing with powders, such sites overlap and are difficult to resolve.

For $m=1$ and $m=2$, negative values of the resonance shift are expressed as $K^{77} = K_s^{77} + K_{orb}^{77}$, where K_s^{77} represents the Knight shift associated with the *s*-contact term, and K_{orb}^{77} is the temperature-independent shift originating from orbital electrons. The Fermi contact term reflects the magnetic coupling of the ^{77}Se nucleus to the *s* character of conduction electrons [15,37], written as $K^{77} = \frac{16\pi}{3} \mu_B^2 \langle |\psi(0)|^2 \rangle_{E_F} N(E_F)$, where μ_B^2 is the Bohr magneton squared, the $\langle |\psi(0)|^2 \rangle_{E_F}$ term is the average probability density at the nucleus for electronic states around the Fermi level (E_F), and $N(E_F)$ is the density of states (DOS) at E_F [36,37,42]. Both samples here are *n*-type semiconductors; hence the sign of the resonance shift is the same for both. However, the $m=1$ sample has a smaller downfield shift than the $m=2$ sample, which means that the carrier density is reduced in this compound relative to the $m=2$ case. To shed light on this divergence, we measured the Seebeck coefficients of these compounds. The $m=1$ sample had a room-temperature Seebeck coefficient value equal to -131 $\mu\text{V/K}$, whereas the value for $m=2$ was -52 $\mu\text{V/K}$. Thus, both samples are *n*-type semiconductors. Similarly, measurements of the carrier density of both $m=1$ and $m=2$ performed by Sassi *et al.* [13] has demonstrated the *n*-type heavily doped nature of these materials.

Combining the semi-classical Mott–Jones formula, according to which the Seebeck coefficient is inversely proportional to the carrier density ($S \sim n^{-\frac{2}{3}}$), with the sign and magnitude of the ^{77}Se Knight shift, which is governed by the Fermi contact term and directly proportional to the density of states (DOS) at the Fermi level (E_F), we conclude that the large ^{77}Se NMR shift reflects the strong coupling between the spin of charge carriers to the magnetic moment of ^{77}Se nuclei via hyperfine interactions. Furthermore, the enhanced ^{77}Se NMR downfield shift of $m=2$ compared to $m=1$ derives mainly from a larger amount of s -character electrons at the Fermi surface of $m=2$ compared to $m=1$.

Lastly, as shown in Fig. 1, the linewidth calculated as full width at half maximum (FWHM) was found to be $\text{FWHM}_{m=1}^{77} = 512 \text{ ppm}$ ($\sim 29 \text{ kHz}$) for $m=1$ and $\text{FWHM}_{m=2}^{77} = 516.89 \text{ ppm}$ ($\sim 30 \text{ kHz}$) for $m=2$. According to the crystallography of these materials [3,4,13,43], a misfit exists between the PbSe and Bi_2Se_3 layers that promotes lattice distortions and gives rise to a distorted octahedral structure, especially near the boundaries. The large carrier density that appears in the $m=2$ sample derives mainly from the doping of Se vacancy, analogous to that of Bi_2Se_3 [3] as well as the presence of antisite defects (Pb/Bi) could also explain the difference or a higher concentration of positively-charged defects in the $m=1$ compound.

In view of the fact that selenium has a nuclear spin of $I=1/2$ and zero nuclear quadrupole moment, the presence of native defects and the aforementioned lattice distortions should not affect the correlation between linewidth behavior and conductivity [9,30]. Moreover, by calculating the ratio of the linewidths of the two compounds, a ratio of 0.99 was found. The calculated ratio [44] of the experimentally measured FWHM is basically associated with the selenium crystallographic site occupancy in the matrix of $(\text{PbSe})_5(\text{Bi}_2\text{Se}_3)_{3m}$. Hence, this finding suggests the presence of an equal number of crystallographic site heterogeneities at the atomic level, as seen by NMR [31,15,16,19,35]. The nearly equal spectrum broadenings that were found is evidence of a structural well ordering of the selenium atoms in the crystal lattice, as well as of a similar amount of possible defects/inhomogeneities in their structure [15,19].

More recently, a comparative crystallographic study by Sassi *et al.* on the same systems suggested that, regardless of m , the mean interatomic distances of Se-Pb atoms remain equal, approximately 3.025 Å for $m=1$ and 3.021 Å for $m=2$ [13]. By using these interatomic distances, we calculated the dipolar coupling constants to be equal to 0.1734 kHz for $m=1$ and 0.1741 kHz for $m=2$, which confirms that the observed line broadening of both compounds cannot be explained by the dipolar broadening and, thus, other contributions play significant role. Based on the abovementioned results, we can now argue that both the Knight shift and FWHM of the spectra correlate with the differences in the density of states of the band structures for $(\text{PbSe})_5(\text{Bi}_2\text{Se}_3)_{3m}$, $m=1,2$, and the single and featureless NMR spectra are due to inhomogeneous Knight shifts of the different Se sites (superposition of ^{77}Se NMR signals) in the lattice [13,43].

To obtain a better understanding of the electronic and structural characteristics of $(\text{PbSe})_5(\text{Bi}_2\text{Se}_3)_{3m}$, $m=1,2$, we also measured the ^{77}Se nuclear spin-lattice relaxation times (T_1) using a saturation recovery method. In non-magnetic degenerate semiconductors, where the Fermi-contact term is sizeable, T_1 probes the Fermi surface. In our case, the Fermi-contact term is dominant and any contribution from dipolar or orbital relaxation terms is negligible. Figure 1b shows the ^{77}Se NMR saturation recovery curves of $m=1$ and 2 at room temperature plotted on a semi-logarithmic scale. We used three kinds of fitting methods to evaluate the spin-lattice relaxation time for both materials. This method is commonly used in inhomogeneous materials [31,45,46]. The experimental data were fitted to the single exponential [31,45], the stretched exponential (where β is the stretching parameter [45,46,47], $0 < \beta < 1$), and the double exponential curve [31]. As shown in Fig. 1, the relaxation recovery curves can be characterized well by both the stretched and the double exponential model. This is evidence of an extended distribution of T_1 times in both samples caused by the different local environments of Se sites, as well as by the local distortion (and lattice mismatch) due to the layered heterostructure.

We first fit the data using the stretched exponential function, where β was found equal to 0.5, independent of temperature. The fit of the experimental data to the stretched exponential curve, shown as solid red line in Fig. 1, gives a spin-lattice relaxation time of 0.41 ± 0.04 s for $m=1$ and 0.24 ± 0.02 s for $m=2$. The obtained T_1 value for $m=2$ is faster than

the relaxation value of $m=1$. However, we note that this model considers a mean T_1 value of all different Se sites without distinguishing between the Se sites in PbSe and Bi₂Se₃ layers. Hence, we further analyzed our data using a double exponential model. This assumes the presence of two different groups of Se sites that exist in the different layers.

The spin-lattice relaxation rate ($1/T_1$) governed by carriers (magnetic interaction) in a semiconducting material [36-38,48] can be expressed as

$$\frac{1}{T_1} = \frac{64\pi}{9} n(T) |\Psi(\text{Se})|^4 \gamma_{\text{Se}}^2 \gamma_e^2 \left(\frac{m^3 kT}{2\pi} \right)^{1/2},$$

where $n(T)$ is the carrier density, which is, according to the equation, a temperature-dependent function and related to the relaxation rate [$n(T) \propto (T_1 T^{\frac{1}{2}})$]. k is the Boltzmann constant, γ_{Se} is the gyromagnetic ratio of ⁷⁷Se, and $|\Psi(\text{Se})|^2$ represents the conduction electron probability density at a selenium nucleus [10,15]. By using the above equation, we can estimate the difference in the carrier density between the two materials. By calculating the $n_{m=1}^{77}(T)$ and $n_{m=2}^{77}(T)$ at ambient temperature, we obtained that $n_{m=2}^{77}(T)$ is two times higher than $n_{m=1}^{77}(T)$. This calculation reveals a remarkable difference in the s -DOS at the Fermi level for these samples. In the recent ARPES study on $m=1$ and $m=2$ samples by Nakayama *et al.*, the authors showed a marked difference of the band dispersions near the Fermi level (E_F) in these two samples [4]. This is in agreement with our observations. Particularly, the band structure for $m=1$ is a single band, whereas for $m=2$ it consists of multiple bands associated with a shallow dip at the top due to the presence of additional bands that cross E_F .

The analysis of the relaxation data with the double exponential function unveiled the presence of two distinct relaxation components across the entire temperature range. We believe that this relaxation model can now represent more appropriately the contributions of the Se groups that are located in the two distinct layers. After extracting the T_1 values for both samples, we plotted the relaxation rates divided by temperature ($1/T_1 T$) as function of temperature (Figure 2a-b), since in non-magnetic semiconductors $1/T_1 T$ provides atomic-level information related to the Fermi surface characteristics [36].

The temperature dependence of the ^{77}Se $1/T_1T$ for $m=1$ ($\text{Pb}_5\text{Bi}_6\text{Se}_{14}$), as shown in Figure 2, follows a complex ^{77}Se NMR relaxation mechanism. The first relaxation component of the double exponential recovery function reveals that, initially, $1/T_1T$ presents a power-law behavior governed by $1/T_1T \sim T^6$ with increasing temperature. This trend may signal the onset of an energy gap quite anisotropic [43]. At high temperatures, $1/T_1T$ increases with temperature before decreasing from 330 K to 420 K. Around 350 K a maximum is achieved. The maximum $1/T_1T$ value is evidence of an increased charge carrier density dominated by electron carriers. An abrupt decrease of $1/T_1T$ for ^{77}Se NMR of $m=1$ is obtained below 350 K. Since $1/T_1T$ is dependent to the density of states, the rapid decrease of $1/T_1T$ is evidence of a (pseudo-) gap opening in the density of states [49,50,51] at the Fermi level of $m=1$. Furthermore, the $1/T_1T$ decreases via a power law ($\sim T^6$). This is a large suppression in $1/T_1T$ that is rarely found in metallic or semiconducting materials, and which exhibits a temperature-independent $1/T_1T$ [36,39,9,49,50,51].

Considering the site-specific sensitivity of NMR relaxivity at the probing nuclear site, such a significant reduction in the $1/T_1T$ clearly suggests a significant change in the density of states [49,50,51]. The reduction in the DOS indicates the opening of a partially spin gapped state with residual density of states at the Fermi energy [9,36,49,50,51,37]. The spin-gap opening begins below 350 K, where the peak temperature of $1/T_1T$ was developed (Fig. 2A). We may also consider that the observed power-law relaxation trend derives from the distribution of the band dispersions near the Fermi level for the $m=1$, which we found to be not purely parabolic, as previously reported [4]. In addition, the complexity of the crystal structure and/or the existence of structural disorder into the matrix may give rise to further complexities [13].

The temperature dependence of the second relaxation component for the $m=1$ was found to be stable across the entire experimental temperature range. A temperature independent $1/T_1T$ confirms the validity of the Korringa relation [36,37,52], $T_1TK_s^2 = \frac{\hbar}{4\pi k_B} \left(\frac{\gamma_e}{\gamma_{Se}} \right)^2 \approx S$ (s -electrons, Korringa constant) due to the scattering of the conduction electrons near the Fermi surface [36,37]. S is the Korringa constant for ^{77}Se , which is equal

to 7.16×10^{-6} sK [53]. Regarding $m=1$, a small value of $1/T_1T=0.005$ s⁻¹K⁻¹ was detected. Comparing the observed value of $m=1$ with the one of a pure Se metal ($1/T_1T=0.15625$ s⁻¹K⁻¹) [54], we can classify $m=1$ as a semiconducting (narrow gap semiconductor-like) material. Furthermore, by taking into consideration the non-linear temperature dependence of the first relaxation component (reduction of DOS at Fermi energy below 350 K, gap opening), we can conclude that the $m=1$ system is a partially gapped semiconductor with finite DOS at the Fermi level. These ⁷⁷Se NMR results agree with Hall mobility data in the same temperature regime [55] reporting a complicated temperature dependence for $m=1$ around 300 K, as well as a significant electron scattering at the interface between PbSe and Bi₂Se₃ layers [13].

The remarkable difference between the band structure of $m=2$ compared to $m=1$ is further revealed by NMR in the temperature dependence of $1/T_1T$ for $m=2$. As shown in Figure 2B, both the short and long relaxation components, as extracted by the double exponential relaxation model, obey the Korringa law [37]. Particularly, in the case of $m=2$, besides the first relaxation rate component (shown in red) that was found to be almost equal to that of $m=1$ ($1/T_1T=0.007$ s⁻¹K⁻¹), the second component (shown in black) follows again the Korringa relation and not a power-law dependence as was the case for $m=1$. However, the extracted $1/T_1T$ for the second component of $m=2$ was 18 times higher ($1/T_1T=0.126$ s⁻¹K⁻¹) than its first component. According to the Korringa expression [36,37]

$$\left(\frac{1}{T_1T}\right)_{\text{metal}} = \frac{4\pi k_B \gamma_{\text{Se}}^2}{\hbar \gamma_e^2} K^2 \propto [N(E_F)]^2,$$

the $\left(\frac{1}{T_1T}\right)_{\text{metal}}$ term is proportional to the square of the density of states at the Fermi level, $N(E_F)$ [36,37]. Therefore, the difference in the two obtained $1/T_1T$ values between the two samples indicates that for the $m=2$ sample the $N(E_F)$ is strongly enhanced relative to $m=1$. Thus, it agrees with the previously reported differences of the band structures between the two samples [4], which mainly arise due to the enhanced band edge crossing around the Fermi level for $m=2$ relative to $m=1$. In addition, our findings are in good agreement with T -dependent electrical resistivity studies [13] that reported a metallic

behavior (electrical resistivity increases with increasing temperature), which tends to saturate at high temperatures in the case of $m=2$ ($60 \mu\Omega.m$). By contrast, in the case of $m=1$ the electrical resistivity is four times higher ($240 \mu\Omega.m$) than that of the $m=2$ compound and a negative temperature coefficient across the entire temperature range (200-400 K).

Furthermore, the observed temperature dependence of $1/T_1T$ for $m=2$ rules out the possibility that the material can be described as a gapped semiconductor (similar to $m=1$), since there is a temperature independence of $1/T_1T$ (Figure 2b). Hence, the dominance of a conducting-electron-caused relaxation mechanism for ^{77}Se nucleus of $m=2$ across the experimental temperature range is apparent in Figure 2B, and aligns with both ARPES [4] and *ab initio* results [8].

More recently, a comparative study by Sassi *et al.* between $m=1$ and $m=2$ systems suggested that the difference between the electronic band structure and conductivity of these two systems is caused by the incorporation of the extra Bi_2Se_3 layer into the matrix [13,55]. The additional Bi_2Se_3 layer sufficiently modifies the electronic band structure by increasing $N(E_F)$, which is in line with the present difference in the NMR spin-lattice relaxation and Knight shift results between $m=1$ and $m=2$. Consequently, crystal structure plays a less pivotal role in the band structure and electrical characteristics of the $(\text{PbSe})_5(\text{Bi}_2\text{Se}_3)_{3m}$ heterostructure than the actual number of Bi_2Se_3 and PbSe layers. Moreover, as Segawa *et al.* [43] suggested for the same materials, the presence of the PbSe layer in the matrix acts as a block layer for the charge transport of the whole system.

The ^{207}Pb NMR spectral (^{207}K , FWHM) characteristics and the ^{207}Pb nuclear spin-lattice relaxation data of both systems were further examined as function of temperature. Figure 3 demonstrates the ^{207}Pb NMR spectra acquired at 260 K from both materials. Both spectra are Gaussian with frequency shifts at 581 ppm ($m=1$) and 638 ppm ($m=2$), whereas the line broadening is well described by a FWHM of 1058 ppm ($m=1$) and 1122 ppm ($m=2$) at 260 K. Figure 4 shows the temperature variation of the ^{207}Pb Knight shift (^{207}K) for $m=1$ and $m=2$ samples. The measured value of ^{207}K for all samples has a positive sign and is nearly independent of temperature below room temperature. However, in Figure 4 the temperature dependence of ^{207}K reveals a marked difference between $m=1$ and $m=2$.

Particularly, in the low temperature regime ($T < 330$ K), ^{207}Pb takes a constant value of approximately 606 ppm for $m=1$ and 645 ppm for $m=2$.

Upon warming above 350 K, the NMR lineshift of $m=2$ becomes temperature dependent and gradually adopts a power-law dependency ($\propto T^{3/2}$). A change in the NMR lineshift above 350 K corresponds to the case of a gapless semiconductor (or semi-metal) mechanism [17,56], as shown in Figure 4-inset. For $m=2$, the aforementioned mechanism seems to be justified by the existence of six dispersive features that cross the Fermi surface between two time-reversal-invariant momenta ($\bar{\Gamma}, \bar{M}$), as also shown in ARPES studies [4]. A similar exponent value has recently been observed in topologically nontrivial Half-Heusler materials due to the orbital diamagnetism induced by enhanced spin-orbit interactions [17,56]. Contrary to $m=2$, the ^{207}Pb of $m=1$ remains constant across the entire experimental temperature range, as expected for semiconducting materials (Fig. 4). We argue that such a striking difference in ^{207}Pb between $m=1$ and $m=2$ originates from the difference in the topology of the band dispersions near the Fermi level that is strongly modified by the addition of a Bi_2Se_3 ($m=\infty$) layer into the matrix, as we have previously detected by ^{77}Se NMR.

More detailed information can be extracted from the analysis of the ^{207}Pb spin-lattice relaxation ($1/T_1$) data. The results of the ^{207}Pb saturation recovery measurements at ambient temperature are shown in Figure 5. The data for both materials are well fitted by a stretched exponential function [45,46,47], where the stretching parameter (β) is presented by the solid line in Fig. 5 (inset). The adequateness of the stretched exponential function is based on the numerous crystallographically-inequivalent Pb sites in the matrix caused by lattice distortion and lattice mismatch along the different layers, regardless of m . The stretching factor takes into account the broad distribution of T_1 over the Pb sites in the samples, and was found temperature independent and equal to $\beta=0.65$ for both materials.

The temperature dependence of ^{207}Pb $1/T_1$ for both materials is reported in Figure 6. In particular, Figure 6 presents semi-logarithmic plots of T_1 versus reciprocal temperature ($1/T$), where the red solid lines represent the thermally activated mechanism [15,48,57], where the linear least-squares fit provides the activation energies of the

relaxation processes for $m=1$ and $m=2$, equal to $E=56.9$ meV (or 660 K) for $m=1$ and 75.7 meV (or 878 K) for $m=2$, respectively. The magnitude of the extracted E for $m=2$ is about 1.3 times higher than that for $m=1$ (Figure 6). The absence of the Korringa law, as opposed to the ^{77}Se NMR results for $m=2$, implies a striking difference in the way that each nucleus (^{77}Se or ^{207}Pb) “feels” the change in the topology of the band structure during the band inversion. Since the spin susceptibility of the electrons around each different nucleus sites (Se and Pb) affects differently the hyperfine field couplings for each nucleus, the $1/T_1$ and Knight shift parameters are not expected to exhibit similar behavior. This site-selective sensitivity of the NMR parameters is an advantage compared to the volume-averaged techniques (e.g. transport, specific heat measurements) [6,9,30,35].

In Figure 6, the higher activation energy detected from ^{207}Pb NMR in Pb sites of $m=2$ coincides with recent band structure calculations [8] of the $m=2$ system, which have shown that Pb bands lie below the Fermi energy and are partially filled with holes around Γ , while there is a gap of approximately 20 meV at the bottom of the Dirac-cone dispersion. Besides the presence of an additional hybridization gap (20 meV) [8,4] around the Fermi level at Γ for $m=2$, charge-density calculations reported that the electrons of Pb atoms are transferred to interstitial regions of the lattice leaving the Pb sites electronically deprived, which is in line with the nonappearance of the Korringa mechanism (i.e. metallicity) in the present ^{207}Pb NMR results (contrary to the ^{77}Se NMR results in $m=2$). Furthermore, the shorter T_1 obtained for $m=1$ in comparison to $m=2$ is a very proof of the higher carrier density surrounding the Pb sites in $m=1$. This can be explained by the swiftness of the spin-lattice relaxation process that is directly related to the number of electrons engaged in the magnetic relaxation channel. Our results, however, do not rule out the possibility that localized defect states may be present in the bandgap region of both $m=1$ and $m=2$. In specific, we found that the extracted activation energies obtained for both compounds match also well the activation energy of 69.2 meV obtained from the ^{207}Pb NMR data in PbSe at the high temperature regime ($T>250$ K) [15]. The larger activation energy detected for the $m=2$ was equal to 75.7 meV and, compared to $m=1$, is closer to the 87 meV activation energy that has been detected via NMR in the high-temperature regime of other topological insulating materials, such as Bi_2Te_3 [18,19]. Additionally, previous studies on PbSe

referred to the presence of localized states varying from 50-70 meV in the bandgap [15,58,59], which is very close to the obtained values in the present study. Hence, the impact of localized defect states in the narrow bandgap region (interband excitations) should be also considered for the interpretation of the topological insulating properties of the $(\text{PbSe})_5(\text{Bi}_2\text{Se}_3)_{3m}$ family. It would be interesting to investigate the relaxation characteristics of the $m>2$ series, as previous studies have reported that both $m=3$ and $m=4$ exhibit similar transport properties despite the additional Bi_2Se_3 layers. Furthermore, the adverse impact of the presence of different types of carriers and native defects on the electronic and thermoelectric characteristics of alloyed ternary and quaternary TIs has been previously demonstrated via NMR and Seebeck coefficient studies [9].

IV. CONCLUSIONS

In conclusion, we investigated the recently discovered topologically nontrivial features at the density of states in the vicinity of the Fermi level of $\text{Pb}_5\text{Bi}_6\text{Se}_{14}$ ($m=1$) and $\text{Pb}_5\text{Bi}_{12}\text{Se}_{23}$ ($m=2$) with ^{77}Se and ^{207}Pb NMR as a function of temperature. Combining the Seebeck coefficient values with the sign and magnitude of the ^{77}Se NMR shifts, the n -type character of these compounds was revealed. In the case of $\text{Pb}_5\text{Bi}_6\text{Se}_{14}$, the ^{207}Pb NMR shifts were found to be temperature independent, while the ^{207}Pb shift for $\text{Pb}_5\text{Bi}_{12}\text{Se}_{23}$ revealed a remarkable enhancement above 350 K following a power-law temperature dependence ($\propto T^{3/2}$), as opposed to the simple semiconducting behavior observed in $\text{Pb}_5\text{Bi}_6\text{Se}_{14}$. Conversely, the ^{77}Se nuclear spin-lattice relaxation rate divided by temperature ($1/T_1T$) yielded a peak around 350 K and then decreased as $1/T_1T \sim T^6$, followed by an almost constant product $1/T_1T$ in the high temperature regime, whereas the second part remained temperature independent. The ^{77}Se NMR relaxation data in $\text{Pb}_5\text{Bi}_{12}\text{Se}_{23}$ for both components are well-described by a free-electron behavior (Korringa law) across the entire temperature range, a signature of the metallic-like properties of this system. Even though the band structure between these two materials differs substantially, the ^{207}Pb NMR relaxation results for both materials follow a thermally activated relaxation pathway, in agreement with the presence of a hybridization gap in the topological states for $m=2$ and

the presence of localized defect states in the bandgap of PbSe [15,58,59] as well as an inhomogeneous distribution of a high defect content in Bi₂Se₃ [31]. Yet, as seen in Figure 6, the resultant activation gaps differ remarkably, being approximately 56.5 meV ($m=1$) and 75.7 meV ($m=2$), because of the different defect level and charge-density at the Pb sites of each compound. The present study clarifies the nature of the heterostructure (PbSe)₅(Bi₂Se₃)_{3 m} family and the effect of its layers on physical properties. This knowledge is relevant for the design of future, heterostructure-based topological materials.

AUTHOR INFORMATION

Corresponding Authors

*Email: dimkoum@chem.ucla.edu (D. K.).

*Email: m-kanatzidis@northwestern.edu (M.K.)

*Email: bouchard@chem.ucla.edu (L.-S. B.).

ACKNOWLEDGMENTS

Work at Argonne (sample preparation, characterization, and crystal growth) is supported by the U.S. DOE, Office of Basic Energy Science, Materials Science and Engineering Division. This research was supported by the Defense Advanced Research Project Agency (DARPA), Award No. N66001-12-1-4034.

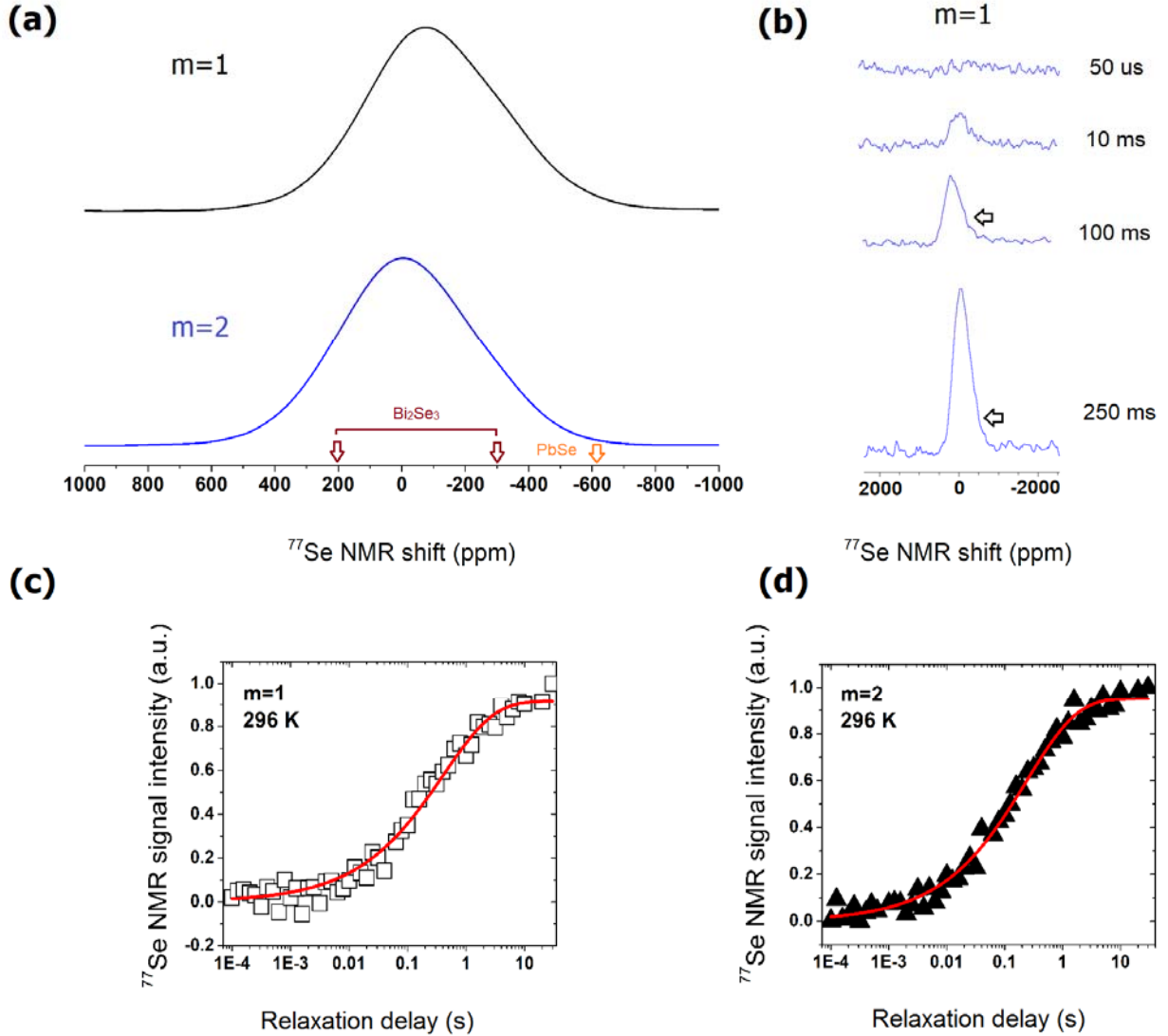


FIG. 1. (a) Static ^{77}Se NMR spectra measurements of $(\text{PbSe})_5(\text{Bi}_2\text{Se}_3)_{3m}$ for $m=1$ and $m=2$, at 7.05 T and at ambient temperature. The positions of the different Se sites are shown on the frequency scale (ppm) for both Bi_2Se_3 and PbSe , as have been reported in Refs. 31,15. (b) The ^{77}Se spectrum for $m=1$ when acquired during the saturation recovery relaxation experiments at different delays (50 μs -250 ms). ^{77}Se magnetization recovery curves of $(\text{PbSe})_5(\text{Bi}_2\text{Se}_3)_{3m}$ for $m=1$ (c) and $m=2$ (d) at 296 K. The solid red line represents a stretched exponential fit.

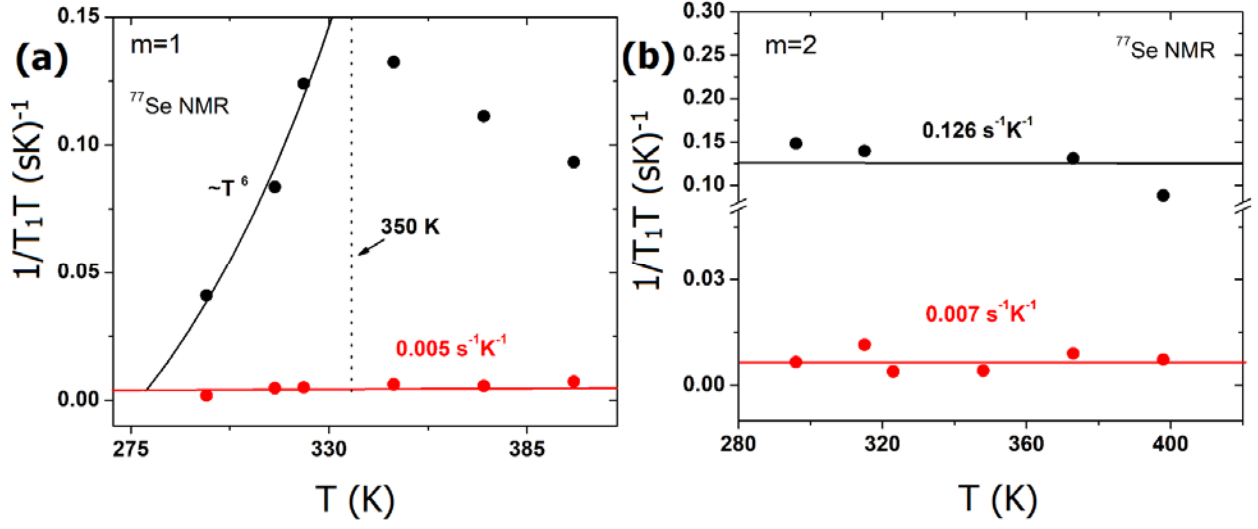


FIG. 2. ^{77}Se nuclear spin-lattice relaxation contributions as function of temperature for $m=1$ ($\text{Pb}_5\text{Bi}_6\text{Se}_{14}$) and $m=2$ ($\text{Pb}_5\text{Bi}_{12}\text{Se}_{23}$), as shown in (a) and (b) respectively. The $1/T_1T$ values were derived by using the double exponential function, as explained in the text. The suppression in the DOS at the Fermi energy (gap opening) is evident in the $m=1$ case (a), as seen by an abrupt decrease of $1/T_1T$ whereas in case of $m=2$ a temperature independent Korringa process holds (typical of gapless behavior) for both relaxation components (b).

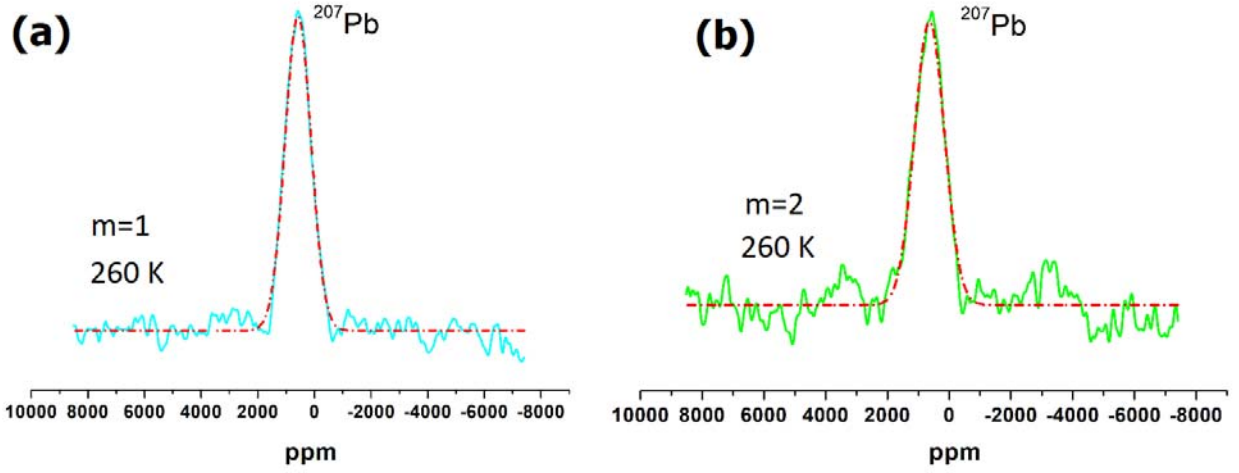


FIG. 3. Solid lines represent ^{207}Pb NMR spectra obtained from $m=1$ (a) and $m=2$ (b) samples of $(\text{PbSe})_5(\text{Bi}_2\text{Se}_3)_{3m}$ at 260 K. The dashed red lines represent Gaussian fit to the data.

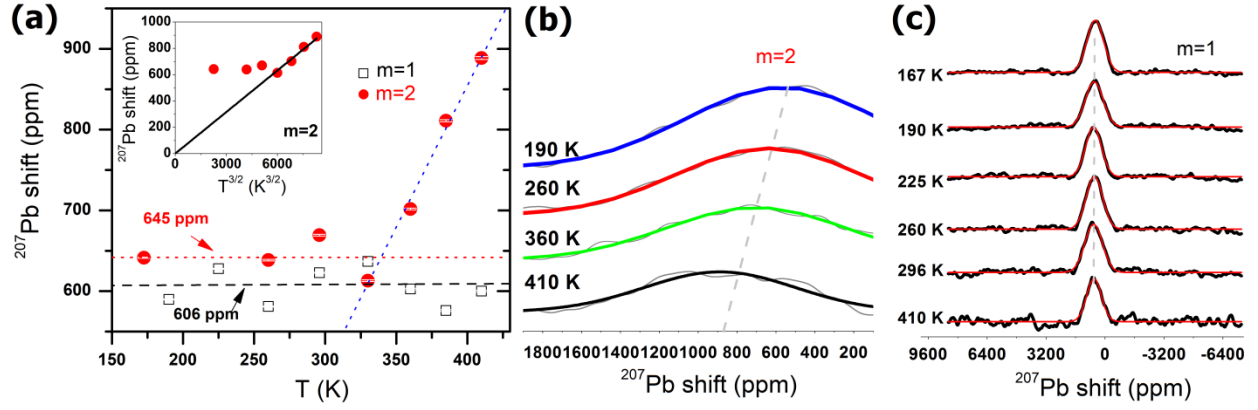


FIG. 4. (a) Temperature dependence of the ^{207}Pb Knight shifts of $(\text{PbSe})_5(\text{Bi}_2\text{Se}_3)_{3m}$, $m=1,2$, where the $m=1$ is shown as black open squares and $m=2$ as red spheres. The inset shows the power-law temperature dependence of the ^{207}Pb shift for the $m=2$ case (red spheres). The remaining two graphs depict the temperature dependence of the ^{207}Pb lineshape for $m=2$ (b) and $m=1$ (c).

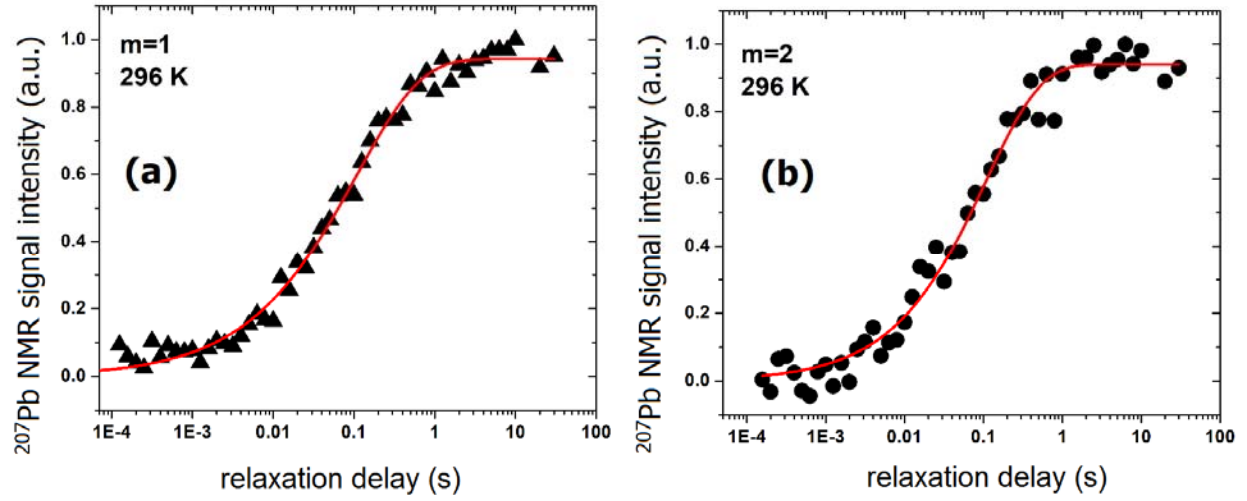


FIG. 5. ^{207}Pb NMR saturation recovery data for $m=1$ (a) and $m=2$ (b) of $(\text{PbSe})_5(\text{Bi}_2\text{Se}_3)_{3m}$ at ambient temperature. The solid red line represents the fit of a stretched exponential model to the recovery data, as described in the text.

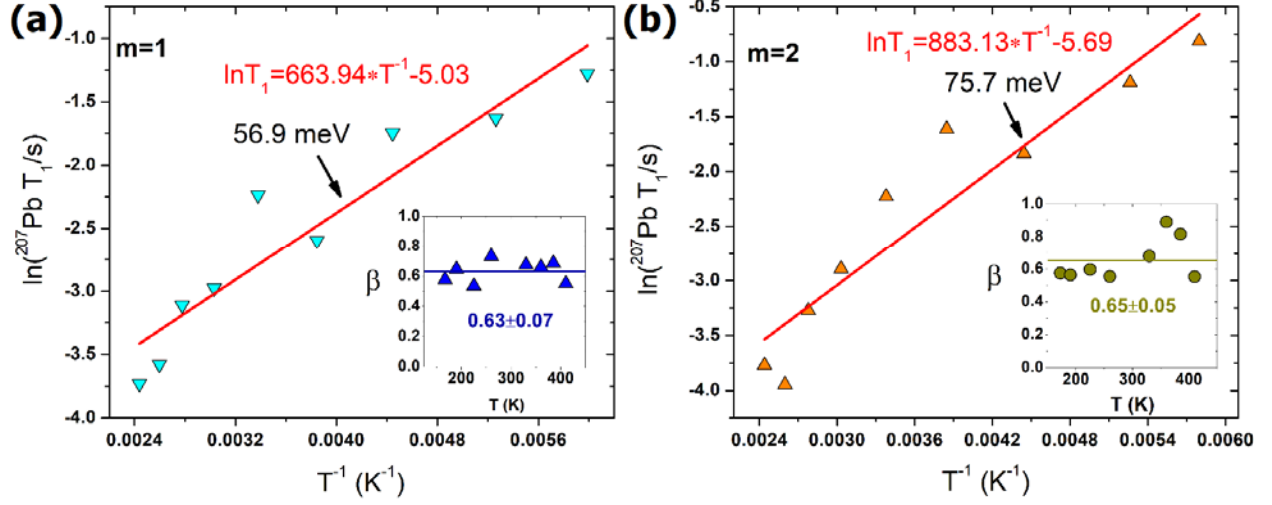


FIG. 6. Semi-logarithmic plot of the ^{207}Pb nuclear spin-lattice relaxation data versus reciprocal temperature for $m=1$ (a) and $m=2$ (b) of $(\text{PbSe})_5(\text{Bi}_2\text{Se}_3)_{3m}$. The solid red line represents a thermal activation mechanism caused by thermally generated mobile carriers, as described in the text. The stretching factors (β) for both materials as function of temperature are shown in the insets.

REFERENCES

- [1] M. G. Kanatzidis, Structural Evolution and Phase Homologies for “Design” and Prediction of Solid-State Compounds, *Acc. Chem. Res.* 38, 359-368 (2005).
- [2] A. Politano, L. Viti, M. S. Vitiello, Optoelectronic devices, plasmonics, and photonics with topological insulators, *APL Materials* 5, 035504 (2017).
- [3] L. Fang, C. C. Stoumpos, Y. Jia, A. Glatz, D. Y. Chung, H. Claus, U. Welp, W.-K. Kwok, M.G. Kanatzidis, Dirac fermions and superconductivity in the homologous structures $(\text{Ag}_x\text{Pb}_{1-x}\text{Se})_5(\text{Bi}_2\text{Se}_3)_{3m}$ ($m=1,2$), *Phys. Rev. B* 90, 020504 (R) (2014).
- [4] K. Nakayama, K. Eto, Y. Tanaka, T. Sato, S. Souma, T. Takahashi, K. Segawa, Y. Ando, Manipulation of Topological States and the Bulk Band Gap Using Natural Heterostructures of a Topological Insulator, *Phys. Rev. Lett.* 109, 236804 (2012).
- [5] Z. Zhu, Y. Cheng, U. Schwingenschlögl, Band inversion mechanism in topological insulators: A guideline for materials design, *Phys. Rev. B* 85, 235401 (2012).
- [6] D. Koumoulis, T.C. Chasapis, B. Leung, R. E. Taylor, C. C. Stoumpos, N. P. Calta, M. G. Kanatzidis, L.-S. Bouchard, Site-Specific Contributions to the Band Inversion in a Topological Crystalline Insulator, *Adv. Electron. Mater.* 1, 1500117 (2015).
- [7] J. O. Dimmock, I. Melngailis, A. J. Strauss, Band Structure and Laser Action in $\text{Pb}_x\text{Sn}_{1-x}\text{Te}$, *Phys. Rev. Lett.*, 16, 1193 (1966).
- [8] H. Momida, G. Bihlmayer, S. Blugel, K. Segawa, Y. Ando T. Oguchi, Topological interface states in the natural heterostructure $(\text{PbSe})_5(\text{Bi}_2\text{Se}_3)_6$ with BiPb defects, *Phys. Rev. B* 97, 035113 (2018).
- [9] T. C. Chasapis, D. Koumoulis, B. Leung, N. P. Calta, S.-H. Lo, V. P. Dravid, L.-S. Bouchard, M. G. Kanatzidis, Two-band model interpretation of the p- to n- transition in ternary tetradymite topological insulators, *APL Mater.* 3, 083601 (2015).

- [10] X. Zhang, Z. Hou, Y. Wang, G. Xu, C. Shi, E. Liu, X. Xi, W. Wang, G. Wu, X. Zhang, NMR Evidence for the Topologically Nontrivial Nature in a Family of Half-Heusler Compounds, *Sci. Rep.* 6, 23172 (2016).
- [11] B. Nowak, D. Kaczorowski, NMR as a Probe of Band Inversion in Topologically Nontrivial Half-Heusler Compounds, *J. Phys. Chem. C* 118, 18021-18026 (2014).
- [12] M. Ohta, D. Y. Chung, M. Kunii, M. G. Kanatzidis, Low lattice thermal conductivity in $\text{Pb}_5\text{Bi}_6\text{Se}_{14}$, $\text{Pb}_3\text{Bi}_2\text{S}_6$, and PbBi_2S_4 : promising thermoelectric materials in the cannizzarite, lillianite, and galenobismuthite homologous series, *J. Mater. Chem. A* 2, 20048-20058 (2014).
- [13] S. Sassi, C. Candolfi, G. Delaizir, S. Migot, J. Ghanbaja, C. Gendarme, A. Dauscher, B. Malaman, B. Lenoir, Crystal Structure and Transport Properties of the Homologous Compounds $(\text{PbSe})_5(\text{Bi}_2\text{Se}_3)_{3m}$ ($m = 2, 3$), *Inorg. Chem.* 57, 422-434 (2018).
- [14] R. K. Harris, B. E. Mann, *NMR and the Periodic Table*, Academic Press, London, 1998.
- [15] D. Koumoulis, R. E. Taylor, D. King, L.-S. Bouchard, NMR study of native defects in PbSe, *Phys. Rev. B* 90, 125201 (2014).
- [16] R. E. Taylor, F. Alkan, D. Koumoulis, M. P. Lake, D. King, C. Dybowski, L.-S. Bouchard, A Combined NMR and DFT Study of Narrow Gap Semiconductors: The Case of PbTe, *J. Phys. Chem. C* 117, 8959-8967 (2013).
- [17] C. Shi, X. Xi, Z. Hou, X. Zhang, G. Xu, E. Liu, W. Wang, W. Wang, J. Chen, G. Wu, NMR investigation of atomic and electronic structures of half-Heusler topologically nontrivial semimetals, *Phys. Status Solidi B* 252, 357-360 (2014).
- [18] D. Koumoulis, T.C. Chasapis, R. E. Taylor, M. P. Lake, D. King, N. N. Jarenwattananon, G. A. Fiete, M. G. Kanatzidis, L.-S. Bouchard, NMR Probe of Metallic States in Nanoscale Topological Insulators, *Phys. Rev. Lett.* 110, 026602 (2013).

- [19] D. Koumoulis, B. Leung, T. C. Chasapis, R. E. Taylor, D. King, M. G. Kanatzidis, L.-S. Bouchard, Understanding Bulk Defects in Topological Insulators from Nuclear-Spin Interactions, *Adv. Funct. Mater.* 24, 1519 (2014).
- [20] R. Guehne, V. Chlan, G. V. M. Williams, S. V. Chong, K. Kadowaki, A. Pöpl, J. Haase, Unusual ^{209}Bi NMR quadrupole effects in topological insulator Bi_2Se_3 , *J. Magn. Res.* 302, 34 (2019).
- [21] B.-L. Young, Z.-Y. Lai, Z. Xu, A. Yang, G. D. Gu, Z.-H. Pan, T. Valla, G. J. Shu, R. Sankar, F. C. Chou, Probing the bulk electronic states of Bi_2Se_3 using nuclear magnetic resonance, *Phys. Rev. B* 86, 075137 (2012).
- [22] D. Koumoulis, R. E. Taylor, J. McCormick, Y. N. Ertas, L. Pan, X. Che, K. L. Wang, L.-S. Bouchard, Effects of Cd vacancies and unconventional spin dynamics in the Dirac semimetal Cd_3As_2 , *J. Chem. Phys.* 147, 084706 (2017).
- [23] D. Koumoulis, G. D. Morris, L. He, X. Kou, D. King, D. Wang, M. D. Hossain, K. L. Wang, G. A. Fiete, M. G. Kanatzidis, L.-S. Bouchard, Nanoscale β -nuclear magnetic resonance depth imaging of topological insulators, *Proc. Natl. Acad. Sci. U S A* 112, E3645-E3650 (2015).
- [24] D. Koumoulis, J. P. Scheifers, R. Touzani, B. P. T. Fokwa, L.-S. Bouchard, Direct chemical fine-tuning of electronic properties in $\text{Sc}_2\text{Ir}_{6-x}\text{Pd}_x\text{B}$, *ChemPhysChem* 17, 2972-2976 (2016).
- [25] D. M. Nisson, N. J. Curro, Nuclear magnetic resonance Knight shifts in the presence of strong spin-orbit and crystal-field potentials, *New J. Phys.* 18, 073041 (2016).
- [26] W. A. MacFarlane, C. B. L. Tschense, T. Buck, K. H. Chow, D. L. Cortie, A. N. Hariwal, R. F. Kiefl, D. Koumoulis, C. D. P. Levy, I. McKenzie, F. H. McGee, G. D. Morris, M. R. Pearson, Q. Song, D. Wang, Y. S. Hor, R. J. Cava, β -detected NMR of $^8\text{Li}^+$ in Bi, Sb, and the topological insulator $\text{Bi}_{0.9}\text{Sb}_{0.1}$, *Phys. Rev. B* 90, 214422 (2014).
- [27] S. Boutin, J. Ramírez-Ruiz, I. Garate, Tight-binding theory of NMR shifts in topological insulators Bi_2Se_3 and Bi_2Te_3 , *Phys. Rev. B* 94, 115204 (2016).

- [28] D. M. Nisson, A. P. Dioguardi, P. Klavins, C. H. Lin, K. Shirer, A. C. Shockley, J. Crocker, N. J. Curro, Nuclear magnetic resonance as a probe of electronic states of Bi_2Se_3 , *Phys. Rev. B* 87, 195202 (2013).
- [29] S. Mukhopadhyay, S. Kramer, H. Mayaffre, H. F. Legg, M. Orlita, C. Berthier, M. Horvatic, G. Martinez, M. Potemski, B. A. Piot, A. Materna, G. Strzelecka, and A. Hruban, Hyperfine coupling and spin polarization in the bulk of the topological insulator Bi_2Se_3 , *Phys. Rev. B* 91, 081105 (2015).
- [30] E.M. Levin, T. M. Riedemann, A. Howard, N. H. Jo, S. L. Bud'ko, P. C. Canfield, T. A. Lograsso, ^{125}Te NMR and Seebeck Effect in Bi_2Te_3 Synthesized from Stoichiometric and Te-Rich Melts, *J. Phys. Chem. C* 120, 44, 25196-25202 (2016).
- [31] R. E. Taylor, B. Leung, M. Lake, L.-S. Bouchard, Spin-Lattice Relaxation in Bismuth Chalcogenides, *J. Phys. Chem. C* 116, 17300-17305 (2012).
- [32] N. M. Georgieva, D. Rybicki, R. Guehne, G. V. M. Williams, S. V. Chong, K. Kadowaki, I. Garate, J. Haase, ^{77}Se nuclear magnetic resonance of topological insulator Bi_2Se_3 , *J. Phys. Rev. B* 93, 195120 (2016).
- [33] K. Matano, M. Kriener, K. Segawa, Y. Ando, G. Zheng, Spin-rotation symmetry breaking in the superconducting state of $\text{Cu}_x\text{Bi}_2\text{Se}_3$, *Nature Physics* 12, 852–854 (2016).
- [34] J. K. Park, C. Y. Lee, C. Kim, NMR probe of bulk electronic structures in H^+ beam irradiated Bi_2Te_3 topological insulator, *Curr. Appl. Phys.* 19, 291-294 (2019).
- [35] E. M. Levin, J. P. Heremans, M. G. Kanatzidis, K. Schmidt-Rohr, Electronic inhomogeneity in n- and p-type PbTe detected by ^{125}Te NMR, *Phys. Rev. B* 88, 115211 (2013).
- [36] D. Wolf, Spin-temperature and nuclear-spin relaxation in matter, Clarendon Press, Oxford, 1979.
- [37] J. Korringa, Nuclear magnetic relaxation and resonance line shift in metals, *Physica* 16, 601 (1950).

- [38] C. S. Lue, B. X. Xie, C. P. Fang, NMR evidence for the coexistence of double structure in CaAlSi, Phys. Rev. B 74, 014505 (2006).
- [39] M. N. Alexander, P. L. Sagalyn, S. D. Senturia, C. R. Hewes, Nuclear spin relaxation study of the electronic structure of lead telluride, J. Nonmetals. 1, 251 (1973).
- [40] M. J. Hirsch, D. F. Holcomb, NMR Study of Si:As and Si:P near the metal-insulator transition, Phys. Rev. B 33, 2520 (1986).
- [41] A. O. Antonenko, D. Y. Nefedov, E. V. Charnaya, S. V. Naumov, V. V. Marchenkov, ^{77}Se Low-Temperature NMR in the Bi_2Se_3 Single Crystalline Topological Insulator, Appl. Magn. Reson. 49(6), 599-605 (2018).
- [42] C. C. Yuan, J. F. Xiang, X. Xi, W. H. Wang, NMR Signature of Evolution of Ductile-to-Brittle Transition in Bulk Metallic Glasses, Phys. Rev. Lett. 107, 236403 (2011).
- [43] K. Segawa, A. A. Taskin, Y. Ando, $\text{Pb}_5\text{Bi}_{24}\text{Se}_{41}$: A new member of the homologous series forming topological insulator heterostructures, J. Solid State Chem. 221,196 (2015).
- [44] The area under an NMR spectrum is proportional to the number of nuclei that resonate within the corresponding frequency window. However, the NMR linewidth not only reflects the distribution of local chemical environments, but is also sensitive to the distribution of native defects, particularly in case of Bi_2Se_3 and PbSe , as already reported in Refs. [15] and [19]. By assuming that $m=1$ and $m=2$ have the same defect density, the ratio of the FWHM will be an indication of the site occupancy between these materials. Two recent studies (See refs. [30] and [34]) have shown that as the defect/vacancy density increases the linewidth also increases (causing an asymmetric lineshape in these TI materials). These studies have shown that defect and/or vacancy regions segregate into domains in both materials. The FWHM of a spectrum represents not only the different selenium sites, but rather mainly the inhomogeneous distribution of the defects with the increased charge carrier concentrations possessing different Knight shifts.

- [45] R. Taylor, P. A. Beckmann, S. Bai, C. Dybowski, ^{127}I and ^{207}Pb Solid-State NMR Spectroscopy and Nuclear Spin Relaxation in PbI_2 : A Preliminary Study, *J. Phys. Chem. C* 118, 17, 9143-9153 (2014).
- [46] D. C. Johnston, Stretched exponential relaxation arising from a continuous sum of exponential decays, *Phys. Rev. B* 74, 184430 (2006).
- [47] D. Bono, J. Hartig, M. Huber, H. Schnockel, L. J. deJongh, ^{27}Al NMR Study of the Metal Cluster Compound $\text{Al}_{50}\text{C}_{120}\text{H}_{180}$, *J. Clust. Sci.* 18, 319–331 (2007).
- [48] M. Shroyer, W. W. Warren, A. I. Ryskin, Nuclear spin-lattice relaxation by optically bistable defects in $\text{CdF}_2\text{:In}$, *Phys. Rev. B* 65, 165202 (2002).
- [49] C. S. Lue, S. H. Yang, T. H. Su, B.-L. Young, NMR evidence for the partially gapped state in $\text{CeOs}_2\text{Al}_{10}$, *Phys. Rev. B* 82, 195129 (2010).
- [50] K. Kang, M. Lee, N. H. Sung, B. K. Cho, Pseudogap opening in single-crystal YMn_4Al_8 investigated through ^{55}Mn and ^{27}Al NMR measurements, *Phys. Rev. B* 98, 224412 (2018).
- [51] C.-S. Lue, J. H. Ross, Pseudogap in Fe_2VGa : NMR evidence, *Phys. Rev. B* 63, 054420 (2001).
- [52] P. Babu, A. Lewera, J. H. Chung, R. Hunger, W. Jaegermann, N. Alonso-Vante, A. Wieckowski, E. Oldfield, Selenium Becomes Metallic in Ru–Se Fuel Cell Catalysts: An EC-NMR and XPS Investigation, *J. Am. Chem. Soc.* 129 (49), 15140-15141 (2007).
- [53] B. S. Zelakiewicz, T. Yonezawa, Y. Tong, Observation of Selenium-77 Nuclear Magnetic Resonance in Octaneselenol-Protected Gold Nanoparticles, *J. Am. Chem. Soc.* 126 (26), 8112 (2004).
- [54] L. L. Lumata, K. Y. Choi, J. S. Brooks, A. P. Reyes, P. L. Kuhns, G. Wu, X. H. Chen, ^{77}Se and ^{63}Cu NMR studies of the electronic correlations in Cu_xTiSe_2 ($x = 0.05, 0.07$), *J. Phys. Condens. Matter.* 22 (29), 295601 (2010).

- [55] S. Sassi, C. Candolfi, V. Ohorodniichuk, C. Gendarme, P. Masschelein, A. Dauscher, B. Lenoir, Thermoelectric Properties of Polycrystalline n-Type $\text{Pb}_5\text{Bi}_6\text{Se}_{14}$. *J. Electron. Mater.* 46, 5 (2017).
- [56] I. M. Tsidilkovski, *Electron Spectrum of Gapless Semiconductors*, Springer Series in Solid-State Sciences, Vol. 116, Springer, New York, 1996.
- [57] G. Neue, S. Bai, R. E. Taylor, P.A. Beckmann, A.J. Vega, C. Dybowski, ^{119}Sn spin-lattice relaxation in $\alpha\text{-SnF}_2$, *Phys. Rev. B* 79, 214302 (2009).
- [58] M. F. Kotkata, M. S. Al-Kotb, I. G. El-Houssieny, Observation of the Meyer-Neldel rule in nanocrystalline PbSe thin films, *Phys. Scr.* 89, 115805 (2014).
- [59] W-F. Li, C-M. Fang, M. Dijkstra, M. A. van Huis, The role of point defects in PbS, PbSe and PbTe: a first principles study, *J. Phys.: Condens. Matter.* 27, 355801 (2015).